

In-situ spectroscopy and shortwave radiometry reveals spatial and temporal variation in the crown-level radiative performance of urban trees

Article

Accepted Version

Creative Commons: Attribution-Noncommercial-No Derivative Works 4.0

Deng, J. ORCID: <https://orcid.org/0000-0001-6896-8622>,
Pickles, B. ORCID: <https://orcid.org/0000-0002-9809-6455> and
Shao, L. ORCID: <https://orcid.org/0000-0002-1544-7548>
(2021) In-situ spectroscopy and shortwave radiometry reveals spatial and temporal variation in the crown-level radiative performance of urban trees. *Remote Sensing of Environment*, 253. 112231. ISSN 0034-4257 doi: 10.1016/j.rse.2020.112231 Available at <https://centaur.reading.ac.uk/94651/>

It is advisable to refer to the publisher's version if you intend to cite from the work. See [Guidance on citing](#).

To link to this article DOI: <http://dx.doi.org/10.1016/j.rse.2020.112231>

Publisher: Elsevier

All outputs in CentAUR are protected by Intellectual Property Rights law, including copyright law. Copyright and IPR is retained by the creators or other copyright holders. Terms and conditions for use of this material are defined in

the [End User Agreement](#).

www.reading.ac.uk/centaur

CentAUR

Central Archive at the University of Reading

Reading's research outputs online

In-situ spectroscopy and shortwave radiometry reveals spatial and temporal variation in the crown-level radiative performance of urban trees

Jie Deng ^{a,*}, Brian J. Pickles ^b, Li Shao ^a

^a School of The Built Environment, University of Reading, Whiteknights, Reading, Berkshire, RG6 6DF, UK

^b School of Biological Sciences, University of Reading, Harborne Building, Whiteknights, Reading RG6 6AS, UK.

* Corresponding author:

E-mail address: j.deng@reading.ac.uk; deng-jie2@163.com (J. Deng)

1 **In-situ spectroscopy and shortwave radiometry reveals spatial and**
2 **temporal variation in the crown-level radiative performance of urban**
3 **trees**

4
5 **Abstract**

6 In conventional microclimate environment modelling, and the development of tree
7 planning strategies for urban heat mitigation, tree crown surface albedo for any given
8 species is assumed to be a constant. However, our recent research into urban tree
9 radiative performance at the crown level implied that tree crown surface albedo changes
10 over time. Based on the in-situ spectroscopy protocols established previously to
11 measure tree crown transfectance, variation in the characteristics of tree crown surface
12 albedo was explored combining spectroscopy and solar shortwave radiometry. Three
13 commonly planted native UK tree species, *Carpinus betulus*, *Acer campestre*, and
14 *Taxus baccata*, were sampled. Spatial distribution profiles of tree crown transfectance
15 measured at fixed solar altitudes were normalised by in-situ spectroradiometry. Tree
16 crown transfectance in the near infrared (NIR) region was found to be proportionally
17 linked to tree crown surface albedo. Within each species, mean tree crown
18 transfectance in the NIR region of 800 – 900 nm was approximately 2.5 times tree
19 crown surface albedo. It was further found that infrared radiation (700–2500 nm)
20 accounted for more than 90% of the total transflected shortwave radiation from tree
21 crowns. The results demonstrate that tree crown surface albedo linearly increases with
22 momentary solar altitude and the maximum tree crown surface albedo corresponds to

23 maximum solar altitude at solar noon on sunny days in summer. Tree crown surface
24 albedo across species tends to be strongly dependent on leaf size if considering visibly
25 dense crown foliage. Our findings provide important insights into tree radiative shading
26 effects resulting from temporal variation in tree crown surface albedo, with
27 consequences for urban microclimate modelling and the development of urban heat
28 mitigation strategies.

29

30 *Keywords:* urban trees; radiative performance; in-situ spectroscopy; infrared radiation;
31 shortwave radiometry; transfectance; tree crown surface albedo; urban microclimate

32 **List of symbols**

Nomenclature	
IRR	solar irradiance, W
IRR_{ref}	solar spectral irradiance on a vertical reference plane, $W/(m^2 \cdot nm)$
$IRR_{SW,incoming}$	incoming shortwave radiation or total solar irradiance, W/m^2
$IRR_{SW,outgoing}$	outgoing shortwave radiation from tree crown, W/m^2
IRR_{VA}	solar spectral irradiance on the surface at a tilted angle of the viewing angle (VA), $W/(m^2 \cdot nm)$
$SF_{\tau R,800-900}$	scale factor of mean transfectance in 800 – 900 nm range to tree crown surface albedo, –
VA	viewing angle of the spectrometer fiber-optic tip relative to horizontal plane, $^{\circ}$
<i>Greek symbols</i>	
α	solar altitude, $^{\circ}$
λ	wavelength, nm
ρ_{albedo}	tree crown surface albedo, –
τR	transfectance of tree crown contour, –
τR_{mean}	mean transfectance in a wavelength interval, –
$\tau R_{mean,800-900}$	mean transfectance in the near infrared region of 800 – 900 nm, –
$\tau R(\lambda)$	spectral transfectance at wavelength λ nm, –
$\tau R_{meas}(\lambda)$	measured spectral transfectance at λ nm wavelength with a vertical reference spectrum, –
$\tau R_{norm}(\lambda)$	normalized spectral transfectance at λ nm wavelength by converting the reference irradiance spectrum in a vertical plane to that in the direction of the viewing angle upwards, –
<i>Abbreviations</i>	
IR	infrared
LAI	leaf area index
NIR	near infrared
UHI	urban heat island
UV	ultraviolet
VIS	visible

34 **1 Introduction**

35 Urban trees play an important role in urban biodiversity, sustainability and climate
36 resilience (Konijnendijk et al., 2005). They can benefit human beings by mitigating heat
37 waves, improving thermal comfort for pedestrians, absorbing carbon dioxide and
38 producing oxygen via photosynthesis, enhancing urban drainage systems and soils,
39 reducing air and noise pollution, providing visual and aesthetic value, and in many other
40 ways (Konijnendijk et al., 2005; Roy et al., 2012). Heat waves have frequently hit many
41 cities globally in the hot summers of the past two decades (Garcia-Herrera et al., 2010;
42 IPCC, 2014; Christidis et al., 2015), leading to high mortality of city dwellers in
43 different countries and regions (Gasparrini and Armstrong, 2011; Guo et al., 2017). In
44 the context of mitigating heat waves and alleviating the effects of global warming,
45 urban trees help to regulate the outdoor thermal environment through evaporative
46 cooling and radiative shading effects (Armson et al., 2013; Wang et al., 2016; Kong et
47 al., 2017; Wu and Chen, 2017; Wang et al., 2018; Tan et al., 2020).

48

49 Research on the benefits of trees for urban heat mitigation has generally focused on the
50 effect of cooling through transpiration, in conjunction with tree physiological
51 conditions, and it has widely been confirmed that urban trees help to mitigate urban
52 heat stress and reduce outdoor temperature in different scenarios and climates (Bowler
53 et al., 2010; Gillner et al., 2015; Lee et al., 2016; Kong et al., 2017; Yang et al., 2017;
54 Zhou et al., 2017; Zhao et al., 2018; Taleghani, 2018; Aminipouri et al., 2019; Wang et

55 al., 2019). Urban trees also have the potential to mitigate Urban Heat Island (UHI)
56 effects (Tan et al., 2016; Jamei et al., 2016; Rahman et al., 2020b). Tree surface
57 temperatures are commonly found to be close to ambient air temperature (within
58 approximately -2 – 5 °C) (Leuzinger et al., 2010; Irmak et al., 2018; Rahman et al.,
59 2020a) in contrast with built surfaces, which tend to be significantly warmer. For
60 example, surface temperatures of sealed ground in an open space are usually 10 to 20 °C
61 warmer than those of trees and green spaces in hot summers (de Abreu-Harbich et al.,
62 2015; Gillner et al., 2015; Speak et al., 2020). It has also been observed that the mean
63 radiant temperature of open fields can be reduced by up to 11 – 30 °C by trees (Gillner
64 et al., 2015; Tan et al., 2017; Zheng et al., 2018; Park et al., 2019). Importantly for urban
65 planning, the tree cooling effect can help to reduce building thermal energy use (Liu
66 and Harris, 2008; Kong et al., 2016; Wang et al., 2016; Hsieh et al., 2018; Tang and
67 Zheng, 2019; Moss et al., 2019), and hence may help to mitigate against increased
68 energy consumption resulting from wider and longer use of air conditioning units. It is
69 widely reported that leaf area index (LAI) is the main driving factor of tree cooling
70 effects (Armson et al., 2013; Rahman et al., 2015; Morakinyo et al., 2018; Zhang et al.,
71 2018), although it should be noted that other, less easily measured, functional traits are
72 rarely considered. In general, tall trees with a large LAI and a wide canopy diameter
73 are suggested to improve the outdoor thermal environment (Kong et al., 2017; Zhang
74 et al., 2018).

75

76 In addition to their role in evaporative cooling, urban trees also contribute to heat
77 mitigation in urban microclimates through radiative shading effects (Georgi and
78 Zafiriadis, 2006; de Abreu-Harbich et al., 2015; Upreti et al., 2017; Wang et al., 2018),
79 whereby shortwave radiation is reflected towards the sky and surrounding surfaces.
80 Upreti *et al.* (2017) simulated the radiative shading effect of urban trees in a regional
81 built environment and predicted that the capacity of trees to reduce urban surface and
82 air temperature was about 2 – 9 °C and 1 – 5 °C, respectively. Monte Carlo ray tracing
83 methods have commonly been used in urban multilayer radiation models to factor in
84 urban tree radiative shading effects with simplified 2D simulation (Krayenhoff et al.,
85 2014; Wang, 2014; Upreti et al., 2017). Essentially, validation of radiative exchange
86 models with trees has been limited due to lack of experimental measurements of
87 radiation within canyons in urban communities (Krayenhoff et al., 2014), which has
88 lead to simplification of modelling approaches. Furthermore, models have typically
89 assumed a spherical leaf angle distribution and a fixed extinction coefficient (e.g. 0.5)
90 for tree intercept radiation (Krayenhoff et al., 2014; Park et al., 2019), meaning that tree
91 radiative performance is modeled as being fixed and invariant with time. Although
92 other microclimate modelling studies have employed complicated 3D CFD
93 (Computational Fluid Dynamics) calculations in ENVI-met with the intention of taking
94 the tree radiative shading effect into account (Wu and Chen, 2017; Eckmann et al., 2018;
95 Zhang et al., 2018; Zhao et al., 2018; Wu et al., 2019), tree crown surface albedo has
96 been considered constant for any given species. Hence, it is important to examine

97 whether these commonly applied assumptions about tree leaves and crowns are in fact
98 correct.

99

100 Generally, previous research into urban microclimate modelling and the development
101 of urban tree planning strategies has used simplified approaches to assess tree radiative
102 shading effects (Lee and Park, 2008; Wang, 2014; Upreti et al., 2017; Zhang et al., 2018;
103 Eckmann et al., 2018; Simon et al., 2018). Tree crown surface albedo for a species is
104 commonly assumed to be a constant in microclimate environment modelling (Eckmann
105 et al., 2018) and in developing urban planning strategies (Zhang et al., 2018); however,
106 temporal variation in tree crown transfectance throughout a day has been demonstrated
107 (Deng et al., 2020). Therefore, to better understand urban tree radiative shading effects,
108 the radiative performance within and between multiple tree species should be examined
109 more closely, especially in the infrared (IR) region.

110

111 Previously, we established a methodology to characterise the IR radiative performance
112 of urban trees by in-situ tree crown spectroscopy (Deng et al., 2019), and employed the
113 method to solve two research questions (Deng et al., 2020): determining the spatial
114 distribution of tree crown transfectance for individual trees, and identifying
115 interspecific differences in tree radiative performance in the IR region. We found that
116 the spatial distribution of a tree's radiative performance varied with solar time and solar
117 altitude, and that interspecific differences in tree radiative performance levels in the IR

118 region were strongly dependent on leaf size in dense foliage (i.e. foliage with no
119 obvious gaps and no concave shapes in tree crown contours) (Deng et al., 2020). Based
120 on this previous work, the present study was designed with the following aims: i) to
121 further identify the spatial distribution profile and temporal variation in tree radiative
122 performance during the northern hemisphere summer by combining in-situ
123 spectroscopy and spectroradiometry, ii) to elucidate the relationship between tree crown
124 mean transfectance in the NIR (Near Infrared) region of 800 – 900 nm and tree crown
125 surface albedo by combining in-situ spectroscopy and shortwave radiometry, and iii) to
126 examine whether temporal variation in the tree crown surface albedo varies across
127 different species. Each of these aims was intended to provide useful information for
128 future urban microclimate modelling and the development of appropriate urban tree
129 planning strategies.

130

131 **2 Measurement methods and test conditions**

132 **2.1 In-situ tree crown spectroscopy and shortwave radiometry**

133 In our previously established protocols for characterising the radiative performance of
134 urban trees (Deng et al., 2019), the term tree crown *transflectance* (τR) or *transflection*
135 was adopted. Here, transflection of shortwave radiation from the tree crown refers to
136 the comprehensive effect of transmitted and reflected shortwave radiation, rather than
137 the individual processes of leaf reflectance or leaf transmittance alone.

138

139 In the present study of tree crown transfectance across species, identical measuring
140 instruments and test facilities were used as in our earlier work (Deng et al., 2020).
141 Namely, a Black-Comet-SR model CXR-SR (StellarNET Inc., Tampa, Florida, USA)
142 concave grating miniature spectrometer (wavelength range: 350 – 1000 nm; spectral
143 resolution: 0.5 nm; field of view of the fiber-optic cable: 25°) was attached to an 8 m
144 tripod to carry out field tests. The tripod was scalable and facilitated raising the
145 spectrometer fiber-optic cable up to a maximum of 8 m and in any direction, as shown
146 in **Figure 1 (a)**. The miniature spectrometer had a spectroradiometer mode for in-situ
147 spectroradiometry; by fitting a cosine receptor to the fiber-optic tip it was able to
148 measure solar irradiance spectra in a field of view of 180° in the measuring wavelength
149 range. Solar irradiance spectra were usually measured synchronously with the tree
150 crown transfectance spectra for normalisation, using the spectroradiometer mode of
151 the miniature spectrometer. Reference spectra in tree crown transfectance
152 measurement were sampled by employing a white reflectance standard RS50 (see
153 **Figure 1 (a)**).

154

155 For the shortwave radiometry, a model SN-500 net radiometer (Apogee Instruments,
156 USA) with a field of view of 150° and calibration uncertainty of $\pm 5\%$ was used to
157 measure four radiation components (incoming shortwave, outgoing shortwave,
158 incoming longwave, outgoing longwave) and net radiation (shortwave and longwave).
159 A model SI-431-SS infrared radiometer (Apogee Instruments, USA) with an ultra-

160 narrow field of view of 28° was used to record tree leaf temperature in the measuring
161 patches in the tree crown. The net radiometer and the infrared radiometer were fixed to
162 a 4.2 m height (adjustable) tripod mast, as shown in **Figure 1 (b)**. As the length of the
163 data communication cable was 4 m, the radiometers could reach a maximum vertical
164 height of 4.2 m. It was not convenient to sample shortwave radiation with the
165 radiometers in different directions due to limitations of the cable length and the tripod
166 mast. As the net radiometer had a field of view of 150° , it was kept 30 – 40 cm away
167 from the sampling patches in the tree crown to guarantee the measurement accuracy.

168



169

(a)

(b)

170

171 **Figure 1.** Deployment of experimental equipment. (a) Miniature spectrometer with a
172 spectroradiometer mode held by a scalable 8 m maximum height tripod for in-situ tree
173 crown spectroscopy; (b) Net radiometer and infrared radiometer fixed on a 4.2 m height
174 (adjustable) tripod mast for in-situ radiometry.

175

176 **2.2 Test conditions**

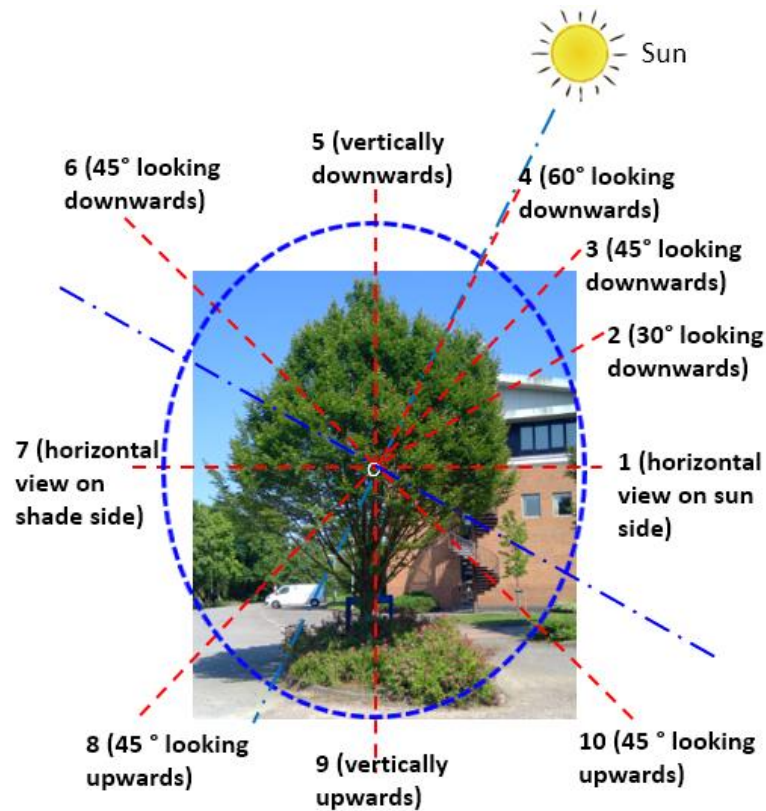
177 Isolated trees of the species *Carpinus betulus* (Fastigate Hornbeam; deciduous), *Acer*
178 *campestre* (Field Maple; deciduous), and *Taxus baccata* (English Yew; evergreen) were
179 sampled in an open field on sunny days in June to August 2020 at the Whiteknights
180 campus, University of Reading (51.44° N, 0.94° W), UK. These species were selected
181 because all three are small to medium sized shade-tolerant trees, native to the UK and
182 Europe, that are commonly planted in urban areas as single trees, groups, or hedgerows
183 (Benham et al., 2016; Sikkema et al., 2016; Zecchin et al., 2016). Operationally, the
184 relatively lower heights of these species, and the ease of access to individuals in open
185 areas, made them very convenient for in-situ tests measuring the spatial distribution of
186 tree crown transfectance. The heights of the sampled trees were in the range of 4.5 –
187 7.0 m. A sampling distance of 2.0 – 5.0 m away from the tree crown contours was
188 chosen in tests. Our earlier tests indicated that a measuring distance of 2.0 – 5.0 m from
189 the tree crown contours to the spectrometer fiber-optic tip was most appropriate for the
190 USB camera, excluded specular reflection from tree leaves, and made the measuring
191 results more robust (Deng et al., 2020). Tree crown transfectance spectra in 350 – 1000
192 nm were sampled in a vertical loop around the tree crown and aligned with the solar
193 azimuth direction (abbreviated as ‘a typically vertical loop’ hereafter) at ten measuring
194 points in different directions (see **Figure 2**). The reference spectrum was always
195 measured in the momentary solar azimuth direction (Deng et al., 2019).

196

197 Conditions of fixed solar altitude were chosen in order to identify the spatial distribution
198 profile of tree radiative performance in terms of the tree crown transreflectance spectra,
199 as it was shown that the spatial distribution of a tree's radiative performance varies
200 temporally with solar altitude (Deng et al., 2020). Scenarios of different solar altitudes
201 were considered to examine temporal variation in tree radiative performance. The tree
202 crown transreflectance spectra in the typically vertical loop were usually sampled from
203 visibly dense foliage with no gaps in the tree crowns in the view vison, though
204 occasionally a concave crown contour appeared in the tree crown. As visibly dense
205 foliage was usually sampled, any background noise signal for the tree crown
206 transreflectance spectra sampling was disregarded according to the demonstration in our
207 earlier work (Deng et al., 2020).

208

209 To determine the relationship between mean tree crown transreflectance in the NIR region
210 and tree crown surface albedo, in-situ spectroscopy and shortwave radiometry were
211 combined. Both the tree crown transreflectance and the solar irradiance spectra were
212 sampled simultaneously using the spectrometer at a point 2.5 – 4.0 m away from the
213 sampled tree crown in a horizontal view, whereas incoming and outgoing shortwave
214 radiation from the tree crown were measured by the net radiometer at a point 30 – 40
215 cm away from the tree crown contour and at the same height as that of the spectrometer
216 sensors.



218

219 **Figure 2.** Illustration of the sampling directions/locations in a vertical loop around the
 220 tree crown and aligned with the solar azimuth direction for an isolated *Carpinus betulus*
 221 in an open space (car park)

222

223 **3 Results and discussion**

224 **3.1 Spatial distribution profile of tree crown transfectance sampled with a vertical** 225 **reference plane**

226 As noted in the test conditions above, fixed solar altitudes were chosen to sample the
 227 tree crown transfectance spectra, employing a vertical reference white plane. Field tests
 228 were implemented for *Carpinus betulus* (Fastigate Hornbeam) and *Acer campestre*

229 (Field Maple) on sunny days between 12:15 – 14:00 (GMT; British Summer Time),
230 when the solar altitude was approximately constant. Ten measuring points in the
231 typically vertical loop around the tree crown aligned with the solar azimuth direction,
232 as illustrated in **Figure 2**, were sampled to identify the spatial distribution profile of
233 tree radiative performance. **Figure 3 (a)** provides the sampled tree crown transfectance
234 spectra of a single *Carpinus betulus* in different directions at solar altitude $\alpha = 61^\circ \pm$
235 1° on 25 June 2020 at Reading, UK. It is evident that the tree crown transfectance
236 spectrum in the IR region with a viewing angle of 60° (point ‘4’) has the highest level,
237 followed in descending order by the IR transfectance spectra with viewing angles of
238 45° (point ‘3’), 30° (point ‘2’), and 90° (point ‘5’). The IR transfectance spectra were
239 at the lowest level in the shade areas (points ‘7’, ‘8’, ‘9’).

240

241 To intuitively display the spatial distribution of tree crown transfectance in the
242 typically vertical loop around the tree crown, mean transfectance in the NIR region of
243 800 – 900 nm ($\tau R_{mean,800-900}$) was adopted as an indicator, because tree crown
244 transfectance spectra in the NIR region (800 – 900 nm) tended to be relatively invariant
245 and held the maximum spectral transfectance in the full wavelength range. The relation
246 of $\tau R_{mean,800-900}$ to tree crown surface albedo will be discussed further in section 3.4.

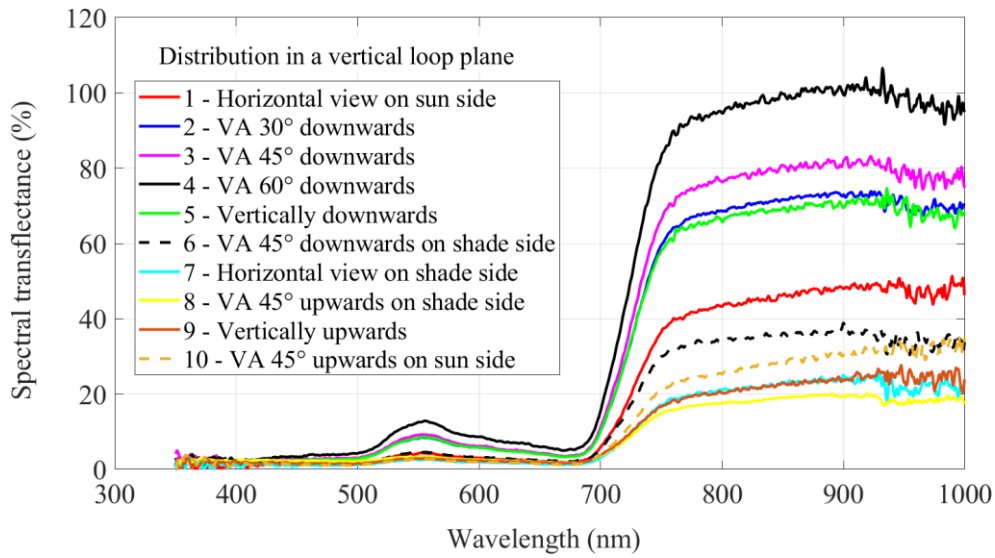
247 **Figure 3 (b)** delineates the spatial distribution profile of tree crown transfectance in
248 the typically vertical loop at solar altitude $\alpha = 61^\circ \pm 1^\circ$ in terms of $\tau R_{mean,800-900}$.
249 Here the mean transfectance ($\tau R_{mean,800-900}$) was approximately symmetric along the

250 axis in the solar altitude direction (noted as ‘symmetric axis’ hereafter). Maximum
251 mean transfectance occurred at point ‘4’ along the symmetric axis (see **Figure 3 (b)**),
252 as the solar irradiance in this direction (i.e. direct normal solar radiation) was larger
253 than in all other directions. This phenomenon was commonly observed for different tree
254 species, as long as the tree crown transfectance spectra were sampled on the patches
255 of tree crowns with visibly dense foliage (i.e. no gaps in foliage, no concave crown
256 contours). It was confirmed in our previous work (Deng et al., 2020) that sparse foliage
257 and concave shapes in the tree crowns degraded the tree crown transfectance levels.

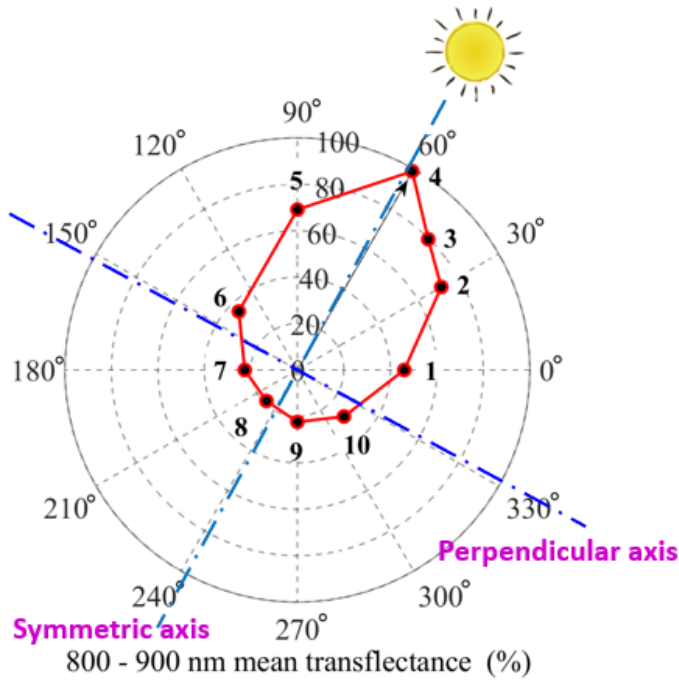
258

259 To better understand the spatial distribution profile of transfectance in **Figure 3 (b)**, it
260 is necessary to introduce another principal axis perpendicular to the symmetric axis
261 (hereafter noted as ‘perpendicular axis’), which aids in distinguishing between
262 characteristics of the transflected radiation in the sunlit area and in the shade area. As
263 sunlight struck the region above the perpendicular axis towards the sky (‘the sunlit
264 area’), transflected radiation from the tree crown in this region was significantly higher
265 than that in the region below the perpendicular axis (‘the shade area’). Since solar
266 radiation only has component vectors in the sunlit area, it is presumed that the
267 transflected shortwave radiation from the tree crown in the sunlit area is dominated by
268 reflected radiation, while the transflected radiation in the shade area is contributed by
269 transmission through multiple layers of tree leaves as well as minor background
270 reflection (e.g. coming from the ground surface or surrounding environment).

271



272 (a)

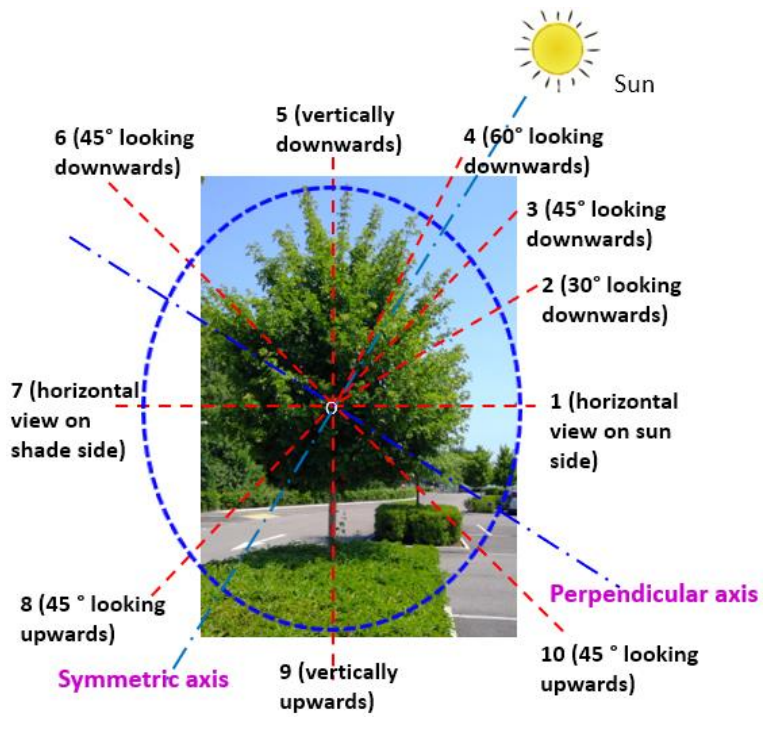


273 (b)

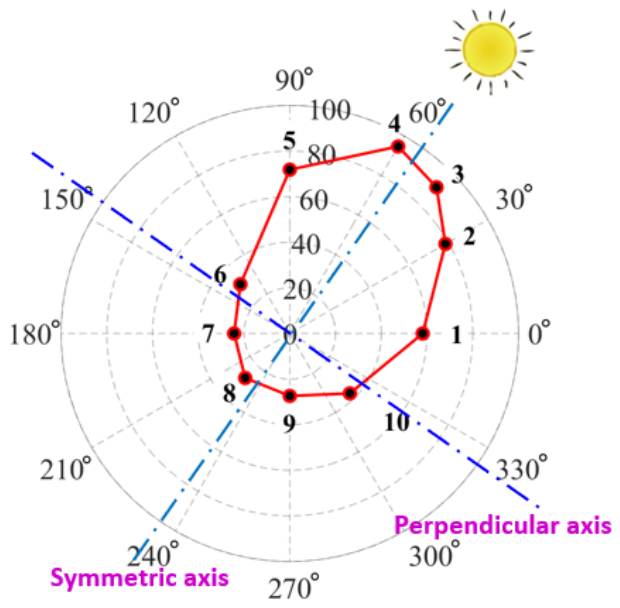
274 **Figure 3.** Test results of a single *Carpinus betulus*. (a) Tree crown transfectance spectra
275 at different sampling directions in the vertical loop around the tree crown in concert
276 with the solar azimuth direction at solar altitude $\alpha = 61^\circ (\pm 1^\circ)$; (b) Spatial distribution
277 profile of the mean transfectance in the NIR region of 800 – 900 nm in the vertical
278 loop

279

280 The approximate symmetry in the spatial distribution profile of mean transreflectance in
281 the 800 – 900 nm range along the symmetric axis of *Carpinus betulus* was also observed
282 in *Acer campestre* and *Taxus baccata*. **Figure 4 (a)** and **(b)** shows an isolated *Acer*
283 *campestre* sampled in an open space and the spatial distribution profile of the mean
284 transreflectance in 800 – 900 nm range in the vertical loop around the tree crown at solar
285 altitude $\alpha = 56^\circ$. The spatial distribution profile was approximately symmetric in the
286 solar altitude direction, except at point ‘6’ where a concave contour appeared in the view
287 vision of the sampling patch in the tree crown (see **Figure 4 (a)**). The concave crown
288 contour degraded the transreflected radiation at point ‘6’. It was also confirmed that for
289 different species, transreflected shortwave radiation from the tree crown in the sunlit area
290 (above the perpendicular axis towards the sky) was dominated by reflection, while that
291 in the shade area (at the lower part of the tree crown below the perpendicular axis) was
292 jointly determined by transmission and minor background reflection.



293 (a)



294 (b) 800 - 900 nm mean transfectance (%)

295 **Figure 4.** Experimental tree and results of spectral measurement. (a) Isolated *Acer*
 296 *campestre* in an open space (car park); (b) Spatial distribution profile of the mean
 297 transfectance in 800 – 900 nm range in the typically vertical loop around the tree crown
 298 at solar altitude $\alpha = 56^\circ$

300 **3.2 Spatial distribution profile of tree radiative performance in terms of** 301 **normalised transfectance in the sunlit area**

302 The tree crown transfectance (τR) spectra sampled at different viewing angles of the
 303 spectrometer fiber-optic tip (VA = 30°, 45°, 60° and 90° looking downwards) with a
 304 vertical reference spectrum can be normalised to equivalent transfectance spectra. This
 305 is achieved by converting the vertical reference irradiance spectra to corresponding
 306 solar irradiance spectra in the incoming solar radiation direction with viewing angles of
 307 the sampled transfectance spectra. The normalised transfectance spectrum is
 308 calculated in **Equation (1)**.

309

$$310 \quad \tau R_{norm}(\lambda) = \tau R_{meas}(\lambda) \cdot IRR_{ref}(\lambda) / IRR_{VA}(\lambda) \quad (1)$$

311

312 **Figure 5 (a)** gives the solar irradiance spectra at different viewing angles (VAs)
 313 synchronously measured at solar altitude $\alpha = 61^\circ$ on the sunny day of 25th June 2020
 314 for normalising the tree crown transfectance in the sunlit area in **Figure 3 (a)**. **Figure**
 315 **5 (b)** displays the normalised transfectance spectra in the sunlit area for the *Carpinus*
 316 *betulus* sampled in the typically vertical loop around the tree crown at solar altitude
 317 $\alpha = 61^\circ (\pm 1^\circ)$. The result indicates that the normalised transfectance spectra at
 318 different viewing angles in the sunlit area turn out to be nearly the same, irrespective of
 319 minor measurement errors due to measuring angle deviation. This mainly occurs

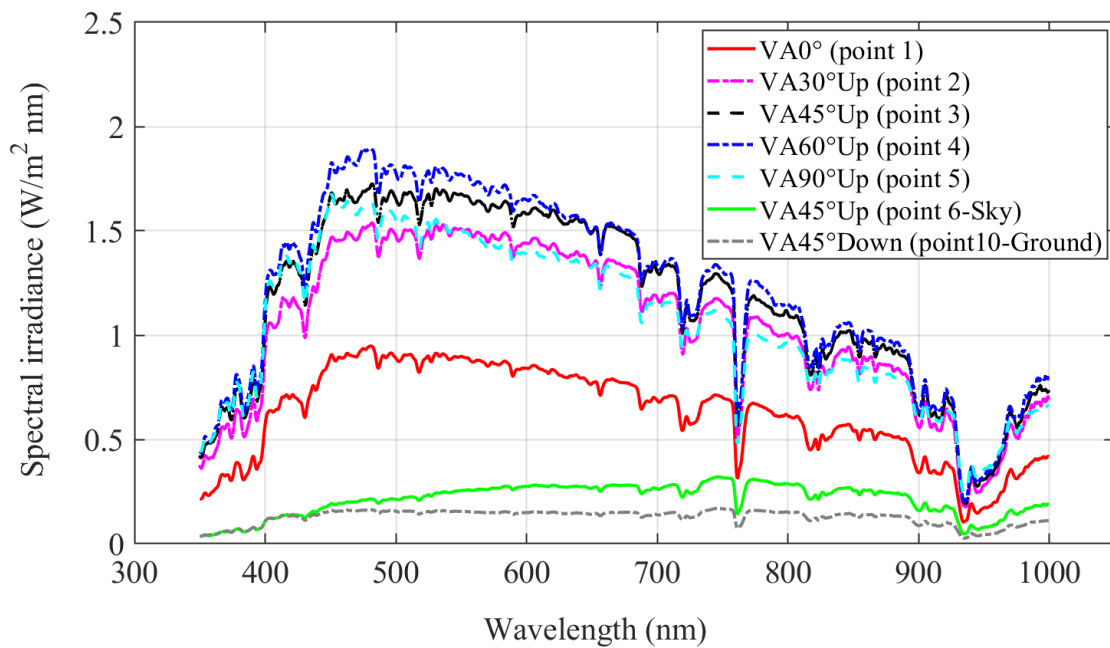
320 because diffuse reflection dominates the tree crown transfection in the sunlit area. It is
321 inferred that measurements taken from sampling patches in the sunlit area with different
322 viewing angles at various heights with visibly dense foliage tends to have nearly the
323 same normalised transfectance. As the momentary solar irradiance in the solar altitude
324 direction is maximum, transflected shortwave radiation from the tree crown in the solar
325 altitude direction turns out to be the greatest compared to other directions, except where
326 gaps in foliage or concave crown contours appear.

327

328 For tree crown transfectance in the shade area, the interaction mechanism was different
329 from that in the sunlit area. Apart from transmitted radiation passing through multiple
330 layers of tree leaves in the tree crown, it was observed that secondary reflected radiation
331 from the lower part of the tree crowns deriving from (sealed or paved) ground surfaces
332 was on the same order of magnitude as the transmitted radiation through leaves. As
333 shown in **Figure 5 (a)**, the magnitude of solar irradiance measuring from point '6'
334 towards the sky was comparable to that from the ground surface to point '10'.
335 Normalising tree crown transfectance consistently at point '6' would result in a much
336 greater transfectance level compared to the normalised transfectance in the sunlit area.
337 Note that point '6' was 74° counterclockwise deviated from the solar altitude at 61° and
338 close to the shade area. It was presumed that point '6' was in the transitional region
339 between the sunlit area and the shade area. Additionally, it did not make sense to
340 normalise the tree crown transfectance in the shade area (points '7', '8', '9', '10') using

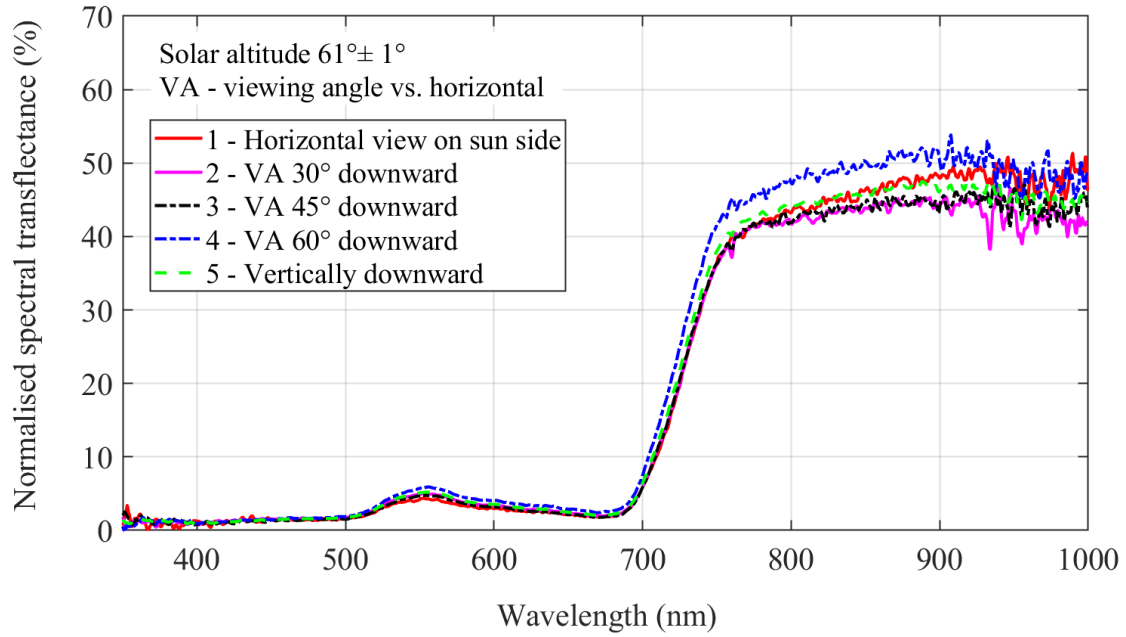
341 background reflected shortwave radiation spectra, because this would lead to much
342 greater transfectance as well. Due to these observations, the vertical reference spectrum
343 was not changed in the normalised spatial distribution profile for the tree crown
344 transfectance in the shade area or in the transitional region between the shade area and
345 the sunlit area.

346



347

348 (a)



349

350 (b)

351 **Figure 5.** Normalisation of tree crown transmittance spectra at different viewing angles.

352 (a) Solar irradiance spectra at different viewing angles; (b) Normalised transmittance

353 spectra of *Carpinus betulus* in the sunlit area

354

355 Based on the transmittance normalisation principle stated above, the spatial distribution

356 profile of tree radiative performance in terms of the normalised transmittance in the

357 sunlit area was obtained via **Equation (1)**. **Figure 6 (a)** displays the spatial distribution

358 of the mean transmittance in the 800 – 900 nm range with normalised transmittance in

359 the sunlit area for the *Carpinus betulus* sampled in the typically vertical loop at solar

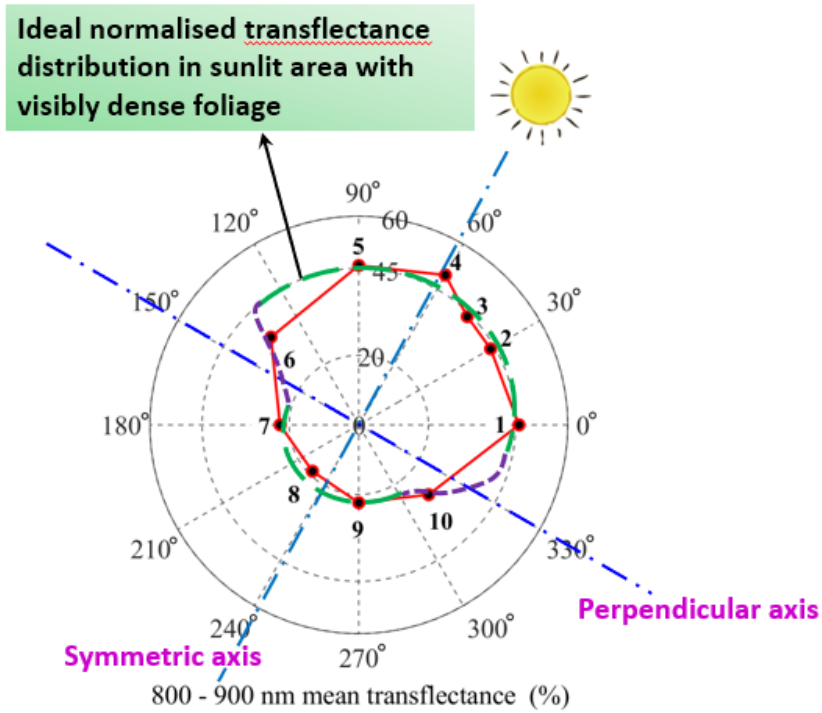
360 altitude $\alpha = 61^\circ (\pm 1^\circ)$, in contrast to the spatial distribution profile with a united

361 vertical reference spectrum in **Figure 3 (b)**. As seen in **Figure 6 (a)**, the normalised

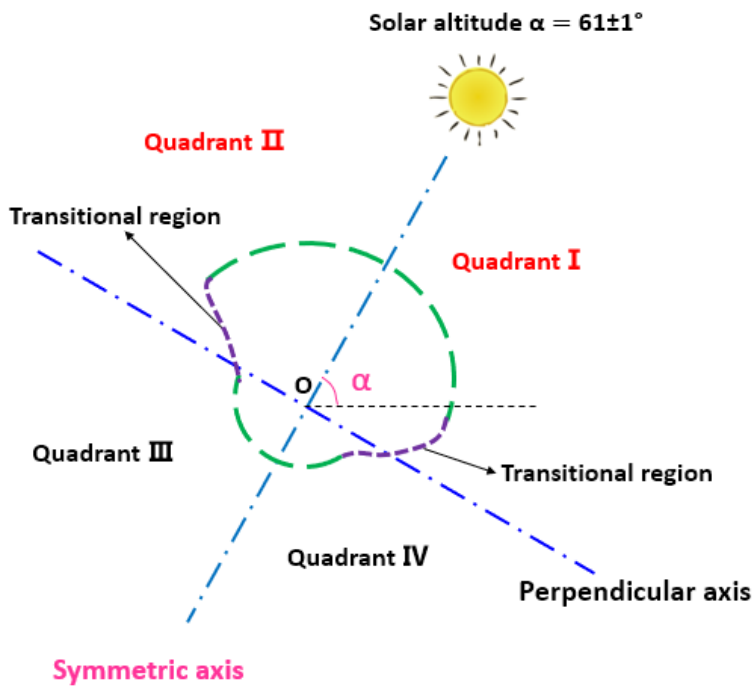
362 mean transmittance in the 800 – 900 nm range in the sunlit area (except point ‘6’ which

363 was close to the shade area and was regarded as being in the transitional region) forms
364 a big circular arc, while the mean transreflectance in the shade area (points '7', '8', '9')
365 forms a relatively smaller circular arc, with transitional regions between the sunlit area
366 and the shade area. The ideal spatial distribution profile and four quadrants of the mean
367 transreflectance in the 800 – 900 nm range were drawn in **Figure 6 (b)**. The ideal profile
368 was determined by experimental data points and understanding of spatial tree radiative
369 performance in terms of IR transreflectance in the sunlit area, the shade area, and the
370 transitional regions. The transreflectance at different viewing angles was normalised in
371 the majority of quadrants I & II (the sunlit area), while the vertical reference spectrum
372 was kept for the transreflectance in quadrants III & IV and the transitional regions. The
373 whole profile looked like a 'mushroom' at a tilted angle of the momentary solar altitude
374 (α). Note that the determination of the ideal mushroom chart was based on normalised
375 transreflectance in the sunlit area with visibly dense foliage being sampled. If there were
376 gaps in foliage or concave shapes in the tree crowns, real distribution profile for
377 individual trees would have local concave shapes compared to the ideal mushroom
378 chart.

379



380 (a)



381 (b)

382 **Figure 6.** (a) Spatial distribution of mean transfectance in the 800 – 900 nm range with
 383 normalised transfectance in the sunlit area for the *Carpinus betulus* tree sampled in the
 384 vertical loop around the tree crown at solar altitude $\alpha = 61^\circ$; (b) Ideal spatial

385 distribution profile and four quadrants of the mean transfectance in 800 – 900 nm range.

386

387 A similar spatial distribution profile of tree radiative performance in terms of

388 normalised transfectance in the sunlit area was also observed in other species. For

389 example, **Figure 7** gives the spatial distribution profile of mean transfectance in 800 –

390 900 nm with normalised transfectance in the sunlit area for the *Acer campestre* (Field

391 Maple) sampled in the typically vertical loop around the tree crown at solar altitude

392 $\alpha = 56^\circ$. It suggests that different species with similar crown morphologies share the

393 common feature of an ideal normalised spatial distribution profile at a fixed solar

394 altitude. For tree species that have different tree crown morphologies (e.g. circle, elliptic,

395 and triangle), to the best of our knowledge, different shapes only lead to differences in

396 the area size of transitional regions (see **Figure 6**) and the arc length of normalised

397 transfectance in the sunlit area. Taking **Figures 6(a)** and **7** as examples, in the

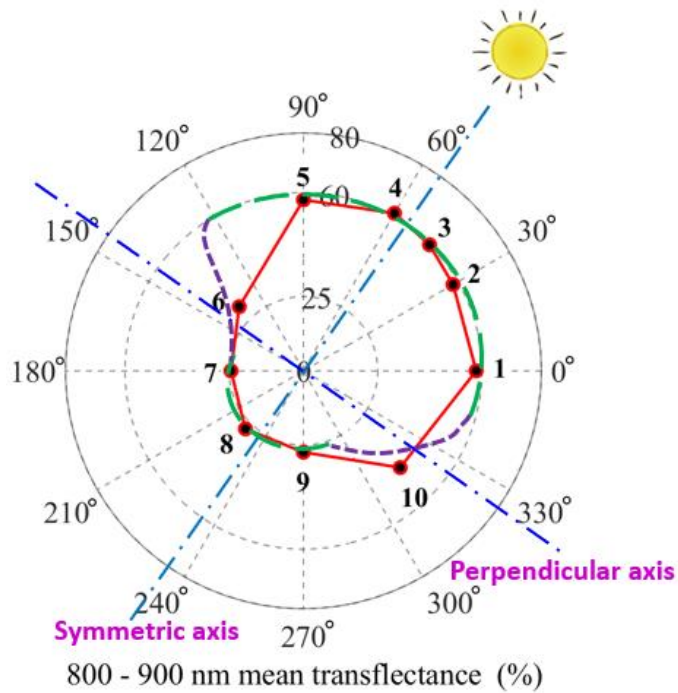
398 measurements of transfectance (red line), we did not measure any locations between

399 points ‘5’ and ‘6’, but if the tree crown was sparse in this area, we can assume that tree

400 crown transfectance in this region would be lower compared to that in the sunlit area.

401 This would result in a shorter arc length of normalised transfectance in the sunlit area.

402



403

404 **Figure 7.** Spatial distribution profile of mean transfectance in 800 – 900 nm based on
 405 the normalised transfectance in the sunlit area for the *Acer campestre* sampled in the
 406 typically vertical loop around the tree crown at solar altitude $\alpha = 56^\circ$

407

408 3.3 Temporal variation of tree radiative performance

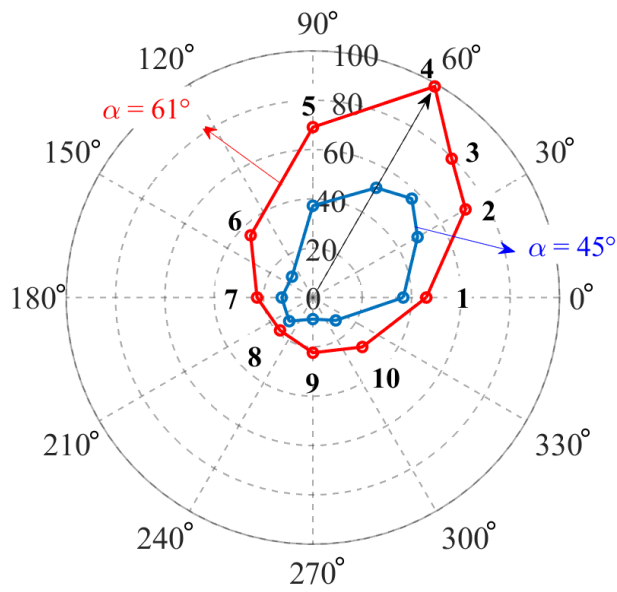
409 As the spatial distribution of tree radiative performance varies with solar altitude (Deng
 410 et al., 2020), temporal variation in the spatial distribution profile of tree crown
 411 transfectance was ascertained. **Figure 8** shows the temporal variation of the
 412 distribution of mean transfectance in the 800 – 900 nm range at two different solar
 413 altitudes $\alpha = 45^\circ$ and 61° for the *Carpinus betulus* sampled in the typically vertical
 414 loop with the vertical reference plane. It suggests that the translected shortwave
 415 radiation from tree crowns at a lower solar altitude (in the morning or afternoon) is

416 significantly lower than that at a higher solar altitude (at or close to solar noon) on a
417 sunny day. To compare the difference quantitatively, the spatial distribution of mean
418 transfectance in 800 – 900 nm sampled at solar altitude 45° is displayed in **Figure 9**
419 **(a)** based on the normalised transfectance in the sunlit area. The normalised mean
420 transfectance in 800 – 900 nm in the sunlit area at solar altitude of 45° was 38.9 %, in
421 contrast to 45.8 % at solar altitude of 61°. The tree crown transfectance in the latter
422 case was increased by 17.9 % compared to the former one. Nevertheless, the spatial
423 distribution profile of the mean transfectance based on the normalised transfectance
424 in the sunlit area tended to be similar at solar altitude $\alpha = 45^\circ$ and $\alpha = 61^\circ$, except
425 that tilted angles of the ‘mushroom chart’ were in concert with the momentary solar
426 altitude (solar time), as shown in **Figure 9 (b)**. The same pattern was noted for different
427 tree species (e.g. compare the normalised distribution profile for *Acer campestre* in
428 **Figure 7** to that of *Carpinus betulus* in **Figure 9**).

429

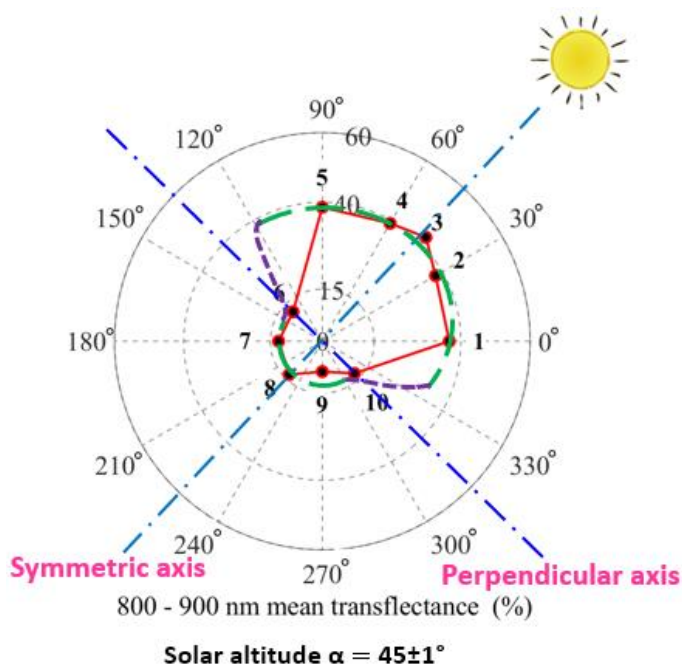
430 Regarding the impact of solar altitude on the tree crown transfectance, our earlier work
431 confirmed that the tree crown transfectance in the IR region within a species in the
432 sunlit area was linearly associated with solar altitude on sunny days (Deng et al., 2020).
433 **Figure 10** provides the mean transfectance (τR) in the 800 – 900 nm range vs. solar
434 altitude (α) for tree species *Carpinus betulus* and *Acer campestre*. Supplementary data
435 for Figure 10 is available in Appendix A.

436



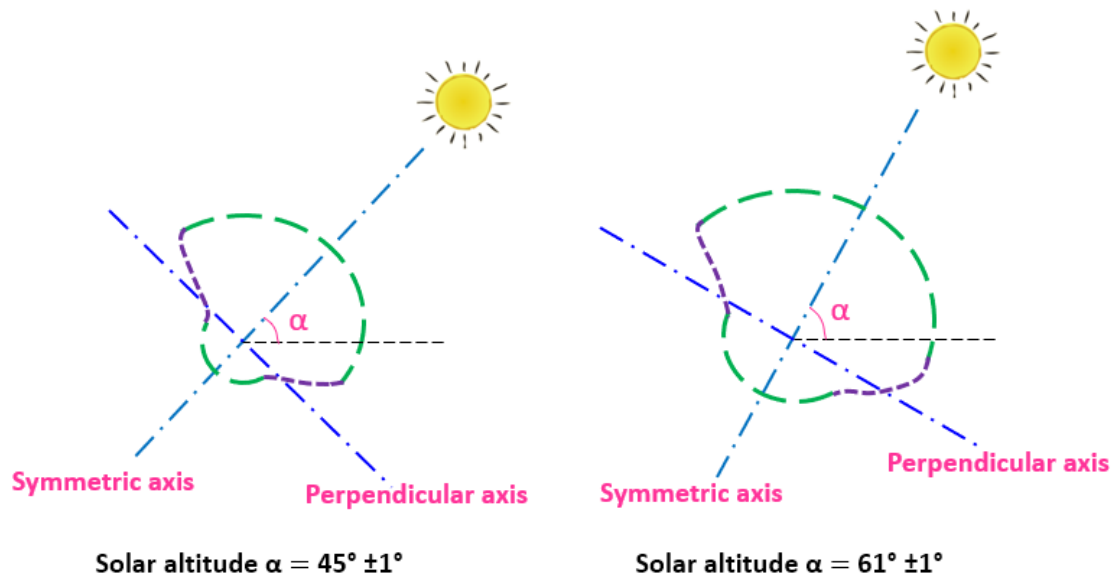
437 800 - 900 nm mean transfectance (%)

438 **Figure 8.** Temporal variation of the distribution of the mean transfectance in 800 –
 439 900nm at two different solar altitudes $\alpha = 45^\circ$ vs. $\alpha = 61^\circ$ for the *Carpinus betulus*
 440 sampled in the typically vertical loop around the tree crown



441

442 (a)

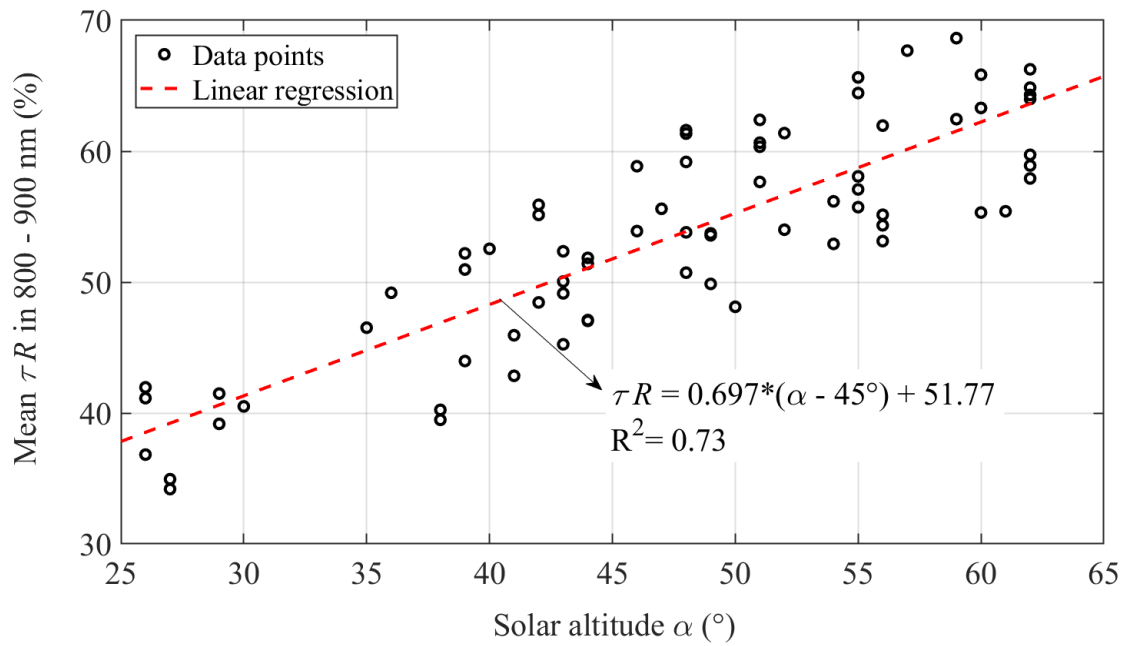
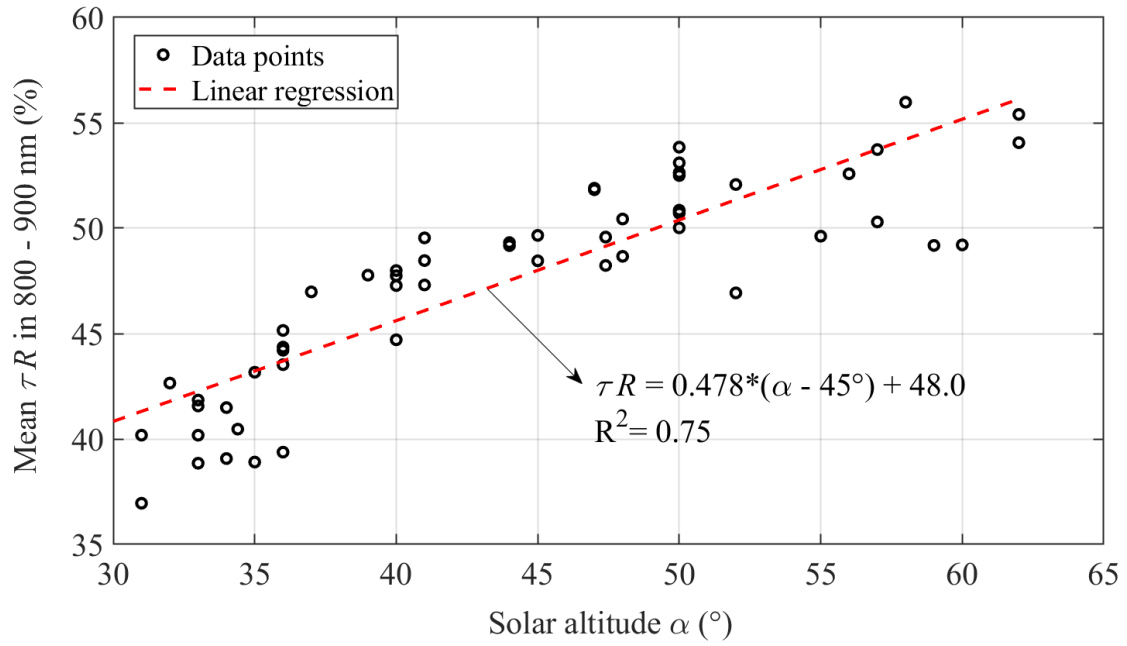


443

444 (b)

445 **Figure 9.** (a) Spatial distribution of mean transfectance in 800 – 900 nm based on
 446 normalised transfectance in the sunlit area for the *Carpinus betulus* sampled in the
 447 typically vertical loop around the tree crown at solar altitude $\alpha = 45^\circ$; (b) Comparison
 448 of spatial distribution profile of the mean transfectance at solar altitude $\alpha = 45^\circ$ and
 449 $\alpha = 61^\circ$

450



455 **Figure 10.** Mean transreflectance (τR) in the 800 – 900 nm range vs. solar altitude (α),
 456 (a) *Carpinus betulus* (Fastigiata hornbeam; slightly different result compared to our
 457 earlier work (Deng et al., 2020) due to addition of extra data collected in summer 2020);

458 (b) *Acer campestre* (Field maple).

459

460 **3.4 Correlating mean transfectance in the 800 – 900 nm range with tree crown** 461 **surface albedo**

462 The tree crown transfectance spectra sampled by in-situ spectroscopy facilitate an
463 understanding of urban tree radiative performance in VIS (visible) and IR regions from
464 the perspective of physical properties. In conventional microclimate environment
465 modelling, tree crown surface albedo is commonly adopted as a constant for a species.

466 The tree crown surface albedo represents the irradiance-weighted total transfectance
467 over the full wavelength range, which may vary with solar time according to spatial
468 variation of the tree crown transfectance. To examine this possibility, we linked the
469 tree crown transfectance spectra to the tree crown surface albedo in the present study.

470 As mean transfectance in the NIR region of 800 – 900 nm ($\tau R_{mean,800-900}$) was
471 adopted as the indicator to demonstrate the spatial distribution profile and temporal
472 variation of urban tree radiative performance in sections 3.1 – 3.3, we explored the
473 underlying mathematical relationship between the $\tau R_{mean,800-900}$ and the tree crown
474 surface albedo. We note that in remote sensing, the tree crown surface albedo could be
475 estimated in a similar manner by linking to the transfectance detected at the top of tree
476 crowns.

477

478 To answer the question, we sampled three tree species, *Carpinus betulus*, *Acer*

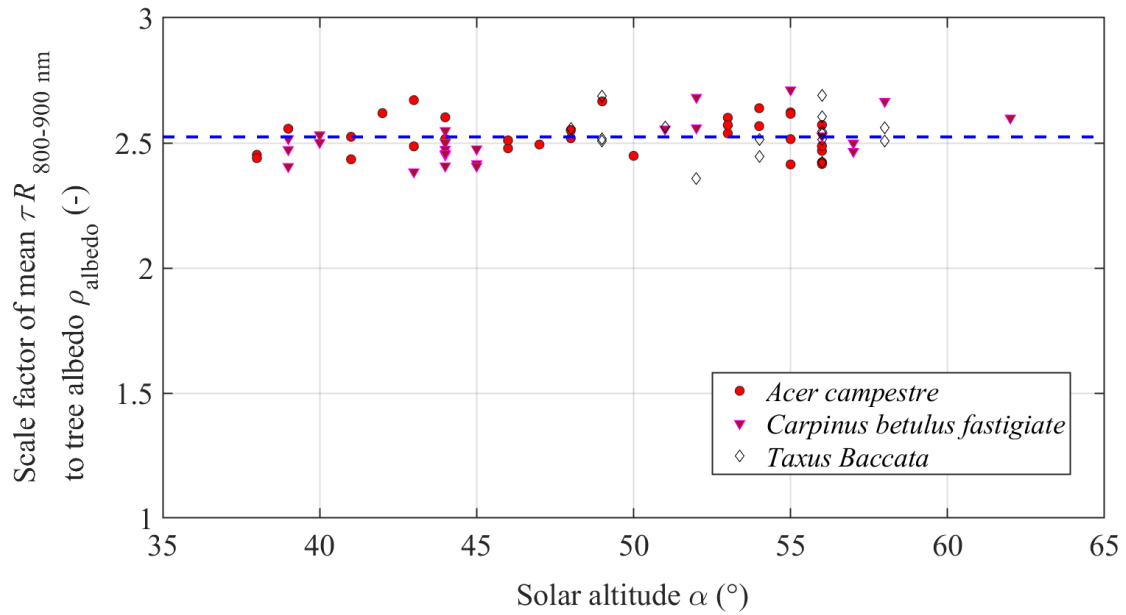
479 *campestris*, and *Taxus baccata* to measure the tree crown transfectance spectra in the
480 wavelength range of 350–1000 nm using a miniature spectrometer with a horizontal
481 view (VA = 0°); we simultaneously recorded the incoming and outgoing shortwave
482 radiation towards tree crowns at the same locations using a net radiometer with the
483 same view angle. The tree crown surface albedo was calculated as the ratio of outgoing
484 shortwave radiation to incoming shortwave radiation, as given in **Equation (3)**. A scale
485 factor of the $\tau R_{mean,800-900}$ to the tree crown surface albedo (ρ_{albedo}) was introduced
486 to explore the mathematical relationship between the two properties, as defined in
487 **Equation (4)**. Based on a combination of in-situ spectroscopy and shortwave
488 radiometry, **Figure 11** shows the scale factor of $\tau R_{mean,800-900}$ to ρ_{albedo} with three
489 tree species (two individual trees for each species) at different solar altitudes. It was
490 found that the mean transfectance in 800 – 900 nm is circa 2.5 times the tree crown
491 surface albedo for the different tree species sampled regardless of the solar altitude,
492 suggesting that the tree crown transfectance in the NIR region is proportionally linked
493 to the tree crown surface albedo.

494

$$495 \quad \rho_{albedo} = \frac{IRR_{SW,outgoing}}{IRR_{SW,incoming}} \quad (3)$$

$$496 \quad SF_{\tau R,800-900} = \frac{\tau R_{mean,800-900}}{\rho_{albedo}} \quad (4)$$

497



498

499 **Figure 11.** Scale factor ($SF_{\tau R,800-900}$) of mean transreflectance in NIR region of 800 –
 500 900 nm ($\tau R_{mean,800-900}$) to the total tree crown contour albedo (ρ_{albedo}) vs. solar
 501 altitude (average $SF_{\tau R,800-900}$ value: 2.52; absolute mean deviation: 2.5 %; root mean
 502 square: 3.2 %)

503

504 To describe the characteristics of the proportional relationship between the mean
 505 transreflectance in 800 – 900 nm and the tree crown surface albedo, it was necessary to
 506 determine the proportion of IR radiation in the total translected shortwave radiation
 507 from tree crowns in the full wavelength range.

508

509 **Figure 12** shows energy decomposition of translected shortwave radiation from the
 510 *Carpinus betulus* tree crown in the UV (ultraviolet), VIS (visible) and IR regions. Both
 511 the tree crown transreflectance and the solar irradiance spectra in 350 –1000 nm were
 512 sampled simultaneously by the spectrometer with a spectroradiometer mode at a point

513 3 m away from the tree crown in a horizontal view, meanwhile the incoming and
514 outgoing shortwave radiation from the tree crown were recorded by the net radiometer
515 at the same location and 30 cm away from the tree crown contour in view of the field
516 of view of the net radiometer. The incoming and outgoing shortwave radiation from the
517 tree crown were 720 W/m^2 and 106.6 W/m^2 , respectively. Hence, the vertical total
518 irradiance was 720 W/m^2 , while the transflected shortwave radiation at the sampling
519 point from tree crown was 106.6 W/m^2 , resulting in a tree surface albedo of 0.148
520 ($=106.6/720$). To simplify the energy decomposition in UV, VIS and IR regions, it was
521 assumed that the UV radiation accounted for 7% of the total irradiance (Duffie and
522 Beckman, 2013) and the mean transfectance in the UV region was the same as that in
523 the 350–500 nm of the VIS region. The assumption in the UV region was plausible, as
524 the proportion of UV radiation to the total solar irradiance in the full wavelength range
525 was relatively small. In terms of energy balance in the full wavelength range for both
526 the total irradiance and the transflected shortwave radiation from the tree crown, two
527 **Equations (5) and (6)** were established with two unknown variables, e.g. solar radiation
528 beyond 1000 nm up to 2500 nm ($IRR_{beyond\ 1000\ nm}$) and the mean transfectance in the
529 IR region beyond 1000 nm ($\tau R_{mean,beyond\ 1000nm}$). In this case, the vertical total solar
530 irradiance of 720 W/m^2 comprised 7.5 W/m^2 of UV radiation, 317 W/m^2 of VIS
531 radiation, 172.7 W/m^2 of NIR radiation, and 179.8 W/m^2 in the IR region beyond 1000
532 nm. Accordingly, the irradiance-weighted mean transfectance in different regions were
533 1.41 %, 2.36 %, 31.7 % and 24.3 %, respectively, in the UV, VIS, NIR, and IR beyond

534 1000 nm regions. It was found that the transflected shortwave radiation in the IR region
535 (700 – 2500 nm) accounted for 92.3% of the total transflected energy in the full
536 wavelength range (300 – 2500 nm) in the measurement at a solar altitude of 45°. For
537 solar altitude in the range of 37° – 58° that we had sampled, it was observed that the
538 transflected shortwave radiation in the IR region accounted for more than 90% of the
539 total transflected energy from the tree crowns in the full wavelength range, meaning
540 that UV and VIS radiation only accounted for a very small proportion of the total
541 transflected energy. The feature of transflected shortwave radiation from the tree crown
542 being dominated by IR radiation explained why the mean transfectance in the NIR
543 region of 800 – 900 nm was directly proportional to the tree crown surface albedo.

544

$$545 \quad IRR_{SW,incoming} = IRR_{UV} + IRR_{VIS,350-700} + IRR_{NIR,700-1000nm} +$$

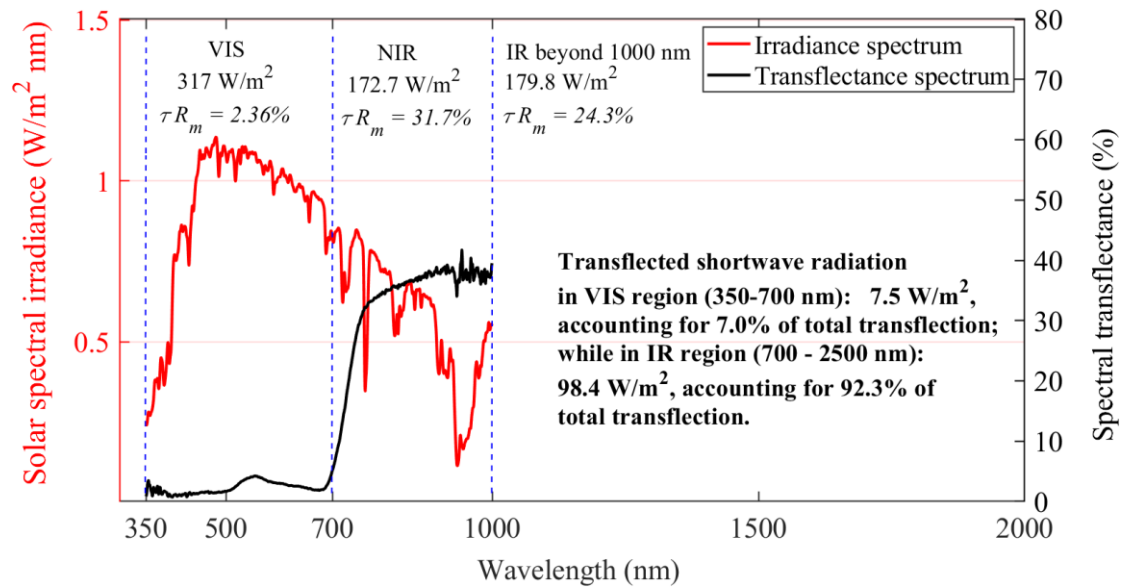
$$546 \quad IRR_{IR,beyond\ 1000\ nm} \quad (5)$$

$$547 \quad IRR_{SW,outgoing} = \tau R_{mean,UV} \cdot IRR_{UV} + \tau R_{mean,350-700nm} \cdot IRR_{VIS,350-700nm} +$$

$$548 \quad \tau R_{mean,700-1000nm} \cdot IRR_{NIR,700-1000nm} + \tau R_{mean,beyond\ 1000nm} \cdot IRR_{beyond\ 1000\ nm}$$

$$549 \quad (6)$$

550



551

552 **Figure 12.** Energy decomposition of transflected shortwave radiation from the

553 *Carpinus betulus* tree crown in UV, VIS, IR regions (tested on 31/07/2020 at 10:33:00,

554 Reading, UK, Solar altitude $\alpha = 45^\circ$; Vertical total irradiance: 720 W/m^2 ; Transflected

555 radiation at the sampling point from tree crown: 106.6 W/m^2 ; ρ_{albedo} : 0.148)

556

557 3.5 Tree crown surface albedo of different species based on the tree crown 558 transflectance measurement

559 After finding in the previous section 3.4 that the mean transflectance in 800 – 900 nm

560 ($\tau R_{mean, 800-900}$) was 2.5 times tree crown surface albedo (ρ_{albedo}) for the three

561 different tree species sampled, the tree crown surface albedo for different species with

562 similar properties was estimated based on tree crown transflectance spectra

563 measurements. Combining the robust linear regression of the $\tau R_{mean, 800-900}$ versus

564 solar altitude for *Carpinus betulus* and *Acer campestre* in **Figure 10 (a)** and **(b)**, the

565 variation of ρ_{albedo} for the two species was given in **Equations (7)** and **(8)**,

566 respectively. It is evident that the tree crown surface albedo linearly increases with solar

567 altitude (α). The maximum tree crown surface albedo corresponds to maximum
568 momentary solar altitude at solar noon.

569

570 For *Carpinus betulus*:

$$571 \quad \rho_{albedo} = \frac{\tau R_{mean,800-900}}{2.5} = 0.191 * (\alpha - 45) + 19.20 \quad (\%) \quad (7)$$

572 For *Acer campestre*:

$$573 \quad \rho_{albedo} = \frac{\tau R_{mean,800-900}}{2.5} = 0.277 * (\alpha - 45) + 20.54 \quad (\%) \quad (8)$$

574

575 Our earlier work used a wide range of in-situ tests to measure the tree crown
576 transfectance across ten tree species commonly planted in the UK (Deng et al., 2020).

577 In terms of the proportional relationship between $\tau R_{mean,800-900}$ and ρ_{albedo}
578 ($SF_{\tau R,800-900} = 2.5$), the tree crown surface albedo for the ten tree species at typical

579 solar altitudes of 30°, 45°, 60° was obtained based on the statistical $\tau R_{mean,800-900}$, as

580 listed in **Table 1**. Furthermore, our earlier work revealed that interspecific differences

581 of tree radiative performance levels in the IR region were strongly dependent on leaf

582 size if only considering visibly dense foliage (i.e. no obvious gaps in foliage and no

583 concave shapes, both of which are common in conifers) in the tree crown contours

584 (Deng et al., 2020). With these caveats, the tree crown surface albedo across multiple

585 tree species tends to be strongly dependent on leaf size. Take the moderate-size leaved

586 species *Acer campestre* and *Quercus robur* as examples to show the difference of tree

587 crown surface albedo at different times on a sunny day in the middle summer (June to

588 middle July in the UK). According to **Table 1**, the tree crown surface albedo at a solar
589 altitude of 60° (near or at noon) for *Acer campestre* and *Quercus robur* trees could be
590 47.0 % and 70.7 % higher than that at a solar altitude of 30° (in the early morning or
591 late afternoon), respectively. Adopting a constant albedo in urban microclimate
592 modelling and in the development of urban tree planning strategies, would probably
593 lead to an incorrect evaluation of the tree radiative shading effects. Hence, temporal
594 variation in tree crown surface albedo with solar time (solar altitude) is an important
595 factor to include in urban microclimate modelling.

596 **Table 1.** Tree crown surface albedo (ρ_{albedo}) at solar altitudes of 30°, 45°, 60° based on the statistical $\tau R_{mean,800-900}$ for ten tree species
 597 commonly planted in the UK

	Solar altitude 30°		Solar altitude 45°		Solar altitude 60°	
Tree species	$\tau R_{mean,800-900}$ (%)	ρ_{albedo} (%)	$\tau R_{mean,800-900}$ (%)	ρ_{albedo} (%)	$\tau R_{mean,800-900}$ (%)	ρ_{albedo} (%)
<i>Sequoiadendron giganteum</i>	32.3 (± 0.7)	12.9 (± 0.3)	38.1 (± 0.8)	15.2 (± 0.3)	43.9 (± 1.0)	17.6 (± 0.3)
<i>Carpinus betulus</i>	39.8 (± 0.7)	15.9 (± 0.3)	46.6 (± 0.8)	18.6 (± 0.3)	53.4 (± 0.9)	21.4 (± 0.3)
<i>Acer campestre</i>	41.5 (± 0.9)	16.6 (± 0.4)	51.2 (± 1.1)	20.5 (± 0.4)	61.0 (± 1.3)	24.4 (± 0.5)
<i>Quercus robur</i>	37.4 (± 0.4)	15.0 (± 0.1)	50.7 (± 0.5)	20.3 (± 0.2)	64.0 (± 0.6)	25.6 (± 0.2)
<i>Platanus x acerifolia</i>	48.5 (± 0.9)	19.4 (± 0.4)	59.8 (± 1.1)	23.9 (± 0.5)	71.2 (± 1.4)	28.5 (± 0.4)
<i>Tilia platyphyllos</i>	34.8 (± 0.7)	13.9 (± 0.3)	49.0 (± 0.9)	19.6 (± 0.4)	63.2 (± 1.2)	25.3 (± 0.4)
<i>Acer x freemanii</i>	35.6 (± 0.4)	14.2 (± 0.2)	47.8 (± 0.6)	19.1 (± 0.2)	60.0 (± 0.7)	24.0 (± 0.2)
<i>Betula pendula</i>	32.2 (± 0.6)	12.9 (± 0.3)	43.8 (± 0.9)	17.5 (± 0.3)	55.3 (± 1.1)	22.1 (± 0.4)
<i>Acer platanoides</i>	40.6 (± 1.3)	16.2 (± 0.5)	55.1 (± 1.5)	22.0 (± 0.6)	69.5 (± 1.9)	27.8 (± 0.7)
<i>Aesculus hippocastanum</i>	45.7 (± 2.2)	18.3 (± 0.9)	59.5 (± 2.9)	23.8 (± 1.2)	73.4 (± 3.6)	29.4 (± 1.1)

598 Note: The '±' values in the brackets denote standard error of the mean. Additional data on mean transfectance in 800 – 900 nm was collected in
599 summer 2020 for the species *Sequoiadendron giganteum*, *Carpinus betulus*, *Acer campestre* and *Acer platanoides*. The values of ρ_{albedo} were
600 based on measurements of visibly dense foliage in tree crowns. For tree species with high incidence of crown gaps and concavities, such as
601 *Sequoiadendron giganteum*, correction factors should be introduced for practice use.

602

603 **4 Conclusions**

604 Using a combination of in-situ spectroscopy and shortwave radiometry for three tree
605 species, *Carpinus betulus*, *Acer campestre*, and *Taxus baccata*, spatial distribution
606 profiles and temporal variation characteristics of the tree crown transfectance were
607 studied. The relationship between mean tree crown transfectance in the NIR region of
608 800 – 900 nm and tree crown surface albedo was demonstrated. The following main
609 conclusions can be drawn:

610 (1) The tree crown transfectance spectra sampled at different viewing angles in the
611 sunlit area can be normalised to an equivalent transfectance spectrum of the
612 same magnitude level, with visibly dense foliage (without obvious gaps in
613 foliage or concave crown contours) in the tree crowns. Tree crown translected
614 shortwave radiation is dominated by reflected radiation in the sunlit area. It is
615 inferred that transfectance measurements of sampling patches in the sunlit area
616 with different viewing angles at various heights with visibly dense foliage tend
617 to have nearly the same normalised transfectance.

618 (2) It was observed that for the different tree species sampled here, the normalised
619 spatial distribution profile of tree crown transfectance in the vertical loop
620 around the tree crown, in concert with the solar azimuth direction, was best
621 described as a ‘mushroom chart’ tilted at an angle of the momentary solar
622 altitude. Note that in the normalised spatial distribution profile, only the

623 transfectance spectra in the sunlit area were normalised, while the
624 transfectance spectra in the shade area and transitional regions were kept with
625 a vertical reference spectrum.

626 (3) Mean tree crown transfectance in the NIR region of 800 – 900 nm was 2.5 times
627 tree crown surface albedo for each of the tree species sampled, suggesting that
628 tree crown transfectance in the NIR region was proportionally linked to tree
629 crown surface albedo. It was observed that the transflected shortwave radiation
630 in the IR region accounted for more than 90% of the total transflected radiation
631 energy from tree crowns in the full wavelength range.

632 (4) Tree crown surface albedo varies with solar time and linearly increases with
633 solar altitude for all measured species. The tree crown surface albedo at solar
634 altitudes of 30°, 45°, and 60° for ten tree species commonly planted in the UK
635 was obtained, based on the proportional relationship between $\tau R_{mean,800-900}$
636 and ρ_{albedo} , as well as tree crown transfectance measurements. The tree crown
637 surface albedo across multiple tree species tends to be strongly dependent on
638 leaf size if considering tree crown contours with visibly dense foliage. Using
639 the moderate-size leaved species *Acer campestre* and *Quercus robur* as
640 examples to show the temporal variation of tree crown surface albedo at
641 different times of the day (based on a sunny day in the middle of summer; June
642 to the middle of July in the UK), we found that tree crown surface albedo at a
643 solar altitude of 60° (near or at noon) for *Acer campestre* and *Quercus robur*

644 trees could be 47.0% and 70.7% higher than that at a solar altitude of 30° (in the
645 early morning or late afternoon), respectively. Hence, adopting a constant tree
646 surface albedo that neglects to account for temporal variation will likely lead to
647 large errors in evaluation of the tree radiative shading effects when modelling
648 the impact of trees on urban microclimates and/or developing urban tree
649 planning strategies.

650

651 The present study has provided important insights into the crown-level radiative
652 performance of individual isolated urban trees from multiple species. We note that
653 future work focused on urban trees planted at different densities (e.g, in urban forestry)
654 and in different configurations (e.g. rows, groups) will be a logical next step.

655

656 **Appendix A. Supplementary data**

657 Supplementary data for Figure 10 is uploaded in the online version.

658

659 **Author contribution statements**

660 Jie Deng: Conceptualization, Methodology, Test plan design, Experiment
661 implementation, Data handling, Writing - Original Draft & Editing

662 Brian J. Pickles: Methodology, Test plan design, Test result assessment, Writing -
663 Review & Editing, Funding Acquisition

664 Li Shao: Conceptualization, Methodology, Test plan design, Test result assessment,

665 Writing - Review, Funding Acquisition

666

667 **Declaration of interest**

668 The authors declare that they have no known competing financial interests or
669 personal relationships that could have appeared to influence the work reported in this
670 paper.

671

672 **Acknowledgment**

673 This work was funded by the UKRI EPSRC and NERC as part of the project
674 'InfruTreeCity: Understanding Infrared radiative performance of urban trees for better
675 future city' (Grant No: EP/P023819/1). The authors wish to thank Dr. Stefan T. Smith
676 and Dr. Christos H. Halios for constructive comments on the methodology.

677

678 **References**

679 Aminipouri, M., Rayner, D., Lindberg, F., Thorsson, S., Knudby, A.J., Zickfeld, K.,

680 Middel, A., Krayenhoff, E.S., 2019. Urban tree planting to maintain outdoor
681 thermal comfort under climate change: The case of Vancouver's local climate
682 zones. *Build. Environ.* 158, 226–236.

683 <https://doi.org/10.1016/j.buildenv.2019.05.022>

684 Armson, D., Rahman, M.A., Ennos, A.R., 2013. A comparison of the shading
685 effectiveness of five different street tree species in Manchester, UK. *Arboric.*

686 Urban For. 39, 157–164.

687 Benham, S.E., Houston Durrant, T., Caudullo, G., de Rigo, D., 2016. *Taxus baccata* in
688 Europe: distribution, habitat, usage and threats. *Eur. Atlas For. Tree Species* 183.

689 Bowler, D.E., Buyung-Ali, L., Knight, T.M., Pullin, A.S., 2010. Urban greening to cool
690 towns and cities: A systematic review of the empirical evidence. *Landsc. Urban*
691 *Plan.* 97, 147–155. <https://doi.org/10.1016/j.landurbplan.2010.05.006>

692 Christidis, N., Jones, G.S., Stott, P.A., 2015. Dramatically increasing chance of
693 extremely hot summers since the 2003 European heatwave. *Nat. Clim. Chang.* 5,
694 46–50. <https://doi.org/10.1038/nclimate2468>

695 de Abreu-Harbich, L.V., Labaki, L.C., Matzarakis, A., 2015. Effect of tree planting
696 design and tree species on human thermal comfort in the tropics. *Landsc. Urban*
697 *Plan.* 138, 99–109. <https://doi.org/10.1016/j.landurbplan.2015.02.008>

698 Deng, J., Pickles, B.J., Kavakopoulos, A., Blanusa, T., Halios, C.H., Smith, S.T., Shao,
699 L., 2019. Concept and methodology of characterising infrared radiative
700 performance of urban trees using tree crown spectroscopy. *Build. Environ.* 157,
701 380–390. <https://doi.org/10.1016/j.buildenv.2019.04.056>

702 Deng, J., Pickles, B.J., Smith, S.T., Shao, L., 2020. Infrared radiative performance of
703 urban trees: spatial distribution and interspecific comparison among ten species in
704 the UK by in-situ spectroscopy. *Build. Environ.* 172, 106682.
705 <https://doi.org/10.1016/j.buildenv.2020.106682>

706 Duffie, J.A., Beckman, W.A., 2013. *Solar Engineering of Thermal Processes: Fourth*

707 Edition, *Solar Engineering of Thermal Processes: Fourth Edition*.
708 <https://doi.org/10.1002/9781118671603>

709 Eckmann, T., Morach, A., Hamilton, M., Walker, J., Simpson, L., Lower, S., McNamee,
710 A., Haripriyan, A., Castillo, D., Grandy, S., Kessi, A., 2018. Measuring and
711 modeling microclimate impacts of *Sequoiadendron giganteum*. *Sustain. Cities Soc.*
712 38, 509–525. <https://doi.org/10.1016/j.scs.2017.12.028>

713 Garcia-Herrera, R., Díaz, J., Trigo, R.M., Luterbacher, J., Fischer, E.M., 2010. A review
714 of the european summer heat wave of 2003. *Crit. Rev. Environ. Sci. Technol.* 40,
715 267–306. <https://doi.org/10.1080/10643380802238137>

716 Gasparrini, A., Armstrong, B., 2011. The impact of heat waves on mortality.
717 *Epidemiology*. <https://doi.org/10.1097/EDE.0b013e3181fdcd99>

718 Georgi, N.J., Zafiriadis, K., 2006. The impact of park trees on microclimate in urban
719 areas. *Urban Ecosyst.* 9, 195–209. <https://doi.org/10.1007/s11252-006-8590-9>

720 Gillner, S., Vogt, J., Tharang, A., Dettmann, S., Roloff, A., 2015. Role of street trees in
721 mitigating effects of heat and drought at highly sealed urban sites. *Landsc. Urban*
722 *Plan.* 143, 33–42. <https://doi.org/10.1016/j.landurbplan.2015.06.005>

723 Guo, Y., Gasparrini, A., Armstrong, B.G., Tawatsupa, B., Tobias, A., Lavigne, E., De
724 Sousa Zanotti Stagliorio Coelho, M., Pan, X., Kim, H., Hashizume, M., Honda, Y.,
725 Leon Guo, Y.L., Wu, C.F., Zanobetti, A., Schwartz, J.D., Bell, M.L., Scortichini,
726 M., Michelozzi, P., Punnasiri, K., Li, S., Tian, L., Garcia, S.D.O., Seposo, X.,
727 Overcenco, A., Zeka, A., Goodman, P., Dang, T.N., Van Dung, D., Mayvaneh, F.,

728 Saldiva, P.H.N., Williams, G., Tong, S., 2017. Heat wave and mortality: A
729 multicountry, multicomunity study. *Environ. Health Perspect.* 125, 1–11.
730 <https://doi.org/10.1289/EHP1026>

731 Hsieh, C.M., Li, J.J., Zhang, L., Schwegler, B., 2018. Effects of tree shading and
732 transpiration on building cooling energy use. *Energy Build.* 159, 382–397.
733 <https://doi.org/10.1016/j.enbuild.2017.10.045>

734 IPCC, 2014. *Climate Change 2014: Synthesis Report. Contribution of Working Groups*
735 *I, II and III to the Fifth Assessment Report of the Intergovernmental Panel on*
736 *Climate Change, Ipcc.*

737 Irmak, M.A., Yilmaz, S., Mutlu, E., Yilmaz, H., 2018. Assessment of the effects of
738 different tree species on urban microclimate. *Environ. Sci. Pollut. Res.* 25, 15802–
739 15822. <https://doi.org/10.1007/s11356-018-1697-8>

740 Jamei, E., Rajagopalan, P., Seyedmahmoudian, M., Jamei, Y., 2016. Review on the
741 impact of urban geometry and pedestrian level greening on outdoor thermal
742 comfort. *Renew. Sustain. Energy Rev.* 54, 1002–1017.
743 <https://doi.org/10.1016/j.rser.2015.10.104>

744 Kong, F., Sun, C., Liu, F., Yin, H., Jiang, F., Pu, Y., Cavan, G., Skelhorn, C., Middel,
745 A., Dronova, I., 2016. Energy saving potential of fragmented green spaces due to
746 their temperature regulating ecosystem services in the summer. *Appl. Energy* 183,
747 1428–1440. <https://doi.org/10.1016/j.apenergy.2016.09.070>

748 Kong, L., Lau, K.K.L., Yuan, C., Chen, Y., Xu, Y., Ren, C., Ng, E., 2017. Regulation of

749 outdoor thermal comfort by trees in Hong Kong. *Sustain. Cities Soc.* 31, 12–25.
750 <https://doi.org/10.1016/j.scs.2017.01.018>

751 Konijnendijk, C.C., Nilsson, K., Randrup, T.B., Schipperijn, J., 2005. *Urban forests and*
752 *trees: A reference book*, Springer-Verlag Berlin Heidelberg. Springer-Verlag
753 Berlin Heidelberg, New York. <https://doi.org/10.1007/3-540-27684-X>

754 Krayenhoff, E.S., Christen, A., Martilli, A., Oke, R.T., 2014. A Multi-layer Radiation
755 Model for Urban Neighbourhoods with Trees. *Boundary-Layer Meteorol.* 151,
756 139–178. <https://doi.org/10.1007/s10546-013-9883-1>

757 Lee, H., Mayer, H., Chen, L., 2016. Contribution of trees and grasslands to the
758 mitigation of human heat stress in a residential district of Freiburg, Southwest
759 Germany. *Landsc. Urban Plan.* 148, 37–50.
760 <https://doi.org/10.1016/j.landurbplan.2015.12.004>

761 Leuzinger, S., Vogt, R., Körner, C., 2010. Tree surface temperature in an urban
762 environment. *Agric. For. Meteorol.* 150, 56–62.
763 <https://doi.org/10.1016/j.agrformet.2009.08.006>

764 Liu, Y., Harris, D.J., 2008. Effects of shelterbelt trees on reducing heating-energy
765 consumption of office buildings in Scotland. *Appl. Energy* 85, 115–127.
766 <https://doi.org/10.1016/j.apenergy.2007.06.008>

767 Morakinyo, T.E., Lau, K.K.L., Ren, C., Ng, E., 2018. Performance of Hong Kong's
768 common trees species for outdoor temperature regulation, thermal comfort and
769 energy saving. *Build. Environ.* 137, 157–170.

770 <https://doi.org/10.1016/j.buildenv.2018.04.012>

771 Moss, J.L., Doick, K.J., Smith, S., Shahrestani, M., 2019. Influence of evaporative
772 cooling by urban forests on cooling demand in cities. *Urban For. Urban Green.* 37,
773 65–73. <https://doi.org/10.1016/j.ufug.2018.07.023>

774 Park, C.Y., Lee, D.K., Krayenhoff, E.S., Heo, H.K., Hyun, J.H., Oh, K., Park, T.Y., 2019.
775 Variations in pedestrian mean radiant temperature based on the spacing and size
776 of street trees. *Sustain. Cities Soc.* 48, 1–9.
777 <https://doi.org/10.1016/j.scs.2019.101521>

778 Rahman, M.A., Armson, D., Ennos, A.R., 2015. A comparison of the growth and
779 cooling effectiveness of five commonly planted urban tree species. *Urban Ecosyst.*
780 18, 371–389. <https://doi.org/10.1007/s11252-014-0407-7>

781 Rahman, M.A., Hartmann, C., Moser-Reischl, A., von Strachwitz, M.F., Paeth, H.,
782 Pretzsch, H., Pauleit, S., Rötzer, T., 2020a. Tree cooling effects and human thermal
783 comfort under contrasting species and sites. *Agric. For. Meteorol.* 287, 107947.
784 <https://doi.org/10.1016/j.agrformet.2020.107947>

785 Rahman, M.A., Stratopoulos, L.M.F., Moser-Reischl, A., Zölch, T., Häberle, K.H.,
786 Rötzer, T., Pretzsch, H., Pauleit, S., 2020b. Traits of trees for cooling urban heat
787 islands: A meta-analysis. *Build. Environ.* 170.
788 <https://doi.org/10.1016/j.buildenv.2019.106606>

789 Roy, S., Byrne, J., Pickering, C., 2012. A systematic quantitative review of urban tree
790 benefits, costs, and assessment methods across cities in different climatic zones.

791 Urban For. Urban Green. 11, 351–363. <https://doi.org/10.1016/j.ufug.2012.06.006>

792 Sikkema, R., Caudullo, G., de Rigo, D., 2016. *Carpinus betulus*. Eur. Atlas For. Tree
793 Species. 74–75.

794 Speak, A., Montagnani, L., Wellstein, C., Zerbe, S., 2020. The influence of tree traits
795 on urban ground surface shade cooling. *Landsc. Urban Plan.* 197, 103748.
796 <https://doi.org/10.1016/j.landurbplan.2020.103748>

797 Taleghani, M., 2018. Outdoor thermal comfort by different heat mitigation strategies-
798 A review. *Renew. Sustain. Energy Rev.* 81, 2011–2018.
799 <https://doi.org/10.1016/j.rser.2017.06.010>

800 Tan, P.Y., Wong, N.H., Tan, C.L., Jusuf, S.K., Schmiele, K., Chiam, Z.Q., 2020.
801 Transpiration and cooling potential of tropical urban trees from different native
802 habitats. *Sci. Total Environ.* 705, 135764.
803 <https://doi.org/10.1016/j.scitotenv.2019.135764>

804 Tan, Z., Lau, K.K.L., Ng, E., 2017. Planning strategies for roadside tree planting and
805 outdoor comfort enhancement in subtropical high-density urban areas. *Build.*
806 *Environ.* 120, 93–109. <https://doi.org/10.1016/j.buildenv.2017.05.017>

807 Tan, Z., Lau, K.K.L., Ng, E., 2016. Urban tree design approaches for mitigating daytime
808 urban heat island effects in a high-density urban environment. *Energy Build.* 114,
809 265–274. <https://doi.org/10.1016/j.enbuild.2015.06.031>

810 Tang, M., Zheng, X., 2019. Experimental study of the thermal performance of an
811 extensive green roof on sunny summer days. *Appl. Energy* 242, 1010–1021.

812 <https://doi.org/10.1016/j.apenergy.2019.03.153>

813 Upreti, R., Wang, Z.H., Yang, J., 2017. Radiative shading effect of urban trees on
814 cooling the regional built environment. *Urban For. Urban Green.* 26, 18–24.
815 <https://doi.org/10.1016/j.ufug.2017.05.008>

816 Wang, C., Wang, Z.H., Yang, J., 2018. Cooling Effect of Urban Trees on the Built
817 Environment of Contiguous United States. *Earth's Futur.* 6, 1066–1081.
818 <https://doi.org/10.1029/2018EF000891>

819 Wang, Chenghao, Wang, Z.H., Wang, Chuyuan, Myint, S.W., 2019. Environmental
820 cooling provided by urban trees under extreme heat and cold waves in U.S. cities.
821 *Remote Sens. Environ.* 227, 28–43. <https://doi.org/10.1016/j.rse.2019.03.024>

822 Wang, Z.H., 2014. Monte Carlo simulations of radiative heat exchange in a street
823 canyon with trees. *Sol. Energy* 110, 704–713.
824 <https://doi.org/10.1016/j.solener.2014.10.012>

825 Wang, Z.H., Zhao, X., Yang, J., Song, J., 2016. Cooling and energy saving potentials of
826 shade trees and urban lawns in a desert city. *Appl. Energy* 16, 437–444.
827 <https://doi.org/10.1016/j.apenergy.2015.10.047>

828 Wu, Z., Chen, L., 2017. Optimizing the spatial arrangement of trees in residential
829 neighborhoods for better cooling effects: Integrating modeling with in-situ
830 measurements. *Landsc. Urban Plan.* 167, 463–472.
831 <https://doi.org/10.1016/j.landurbplan.2017.07.015>

832 Wu, Z., Dou, P., Chen, L., 2019. Comparative and combinative cooling effects of

833 different spatial arrangements of buildings and trees on microclimate. *Sustain.*
834 *Cities Soc.* <https://doi.org/10.1016/j.scs.2019.101711>

835 Yang, A.S., Juan, Y.H., Wen, C.Y., Chang, C.J., 2017. Numerical simulation of cooling
836 effect of vegetation enhancement in a subtropical urban park. *Appl. Energy* 192,
837 178–200. <https://doi.org/10.1016/j.apenergy.2017.01.079>

838 Zecchin, B., Caudullo, G., Rigo, D. de, 2016. *Acer campestre* : acero campestre. *Eur.*
839 *Atlas For. Tree Species* 52–53.

840 Zhang, L., Zhan, Q., Lan, Y., 2018. Effects of the tree distribution and species on
841 outdoor environment conditions in a hot summer and cold winter zone: A case
842 study in Wuhan residential quarters. *Build. Environ.* 130, 27–39.
843 <https://doi.org/10.1016/j.buildenv.2017.12.014>

844 Zhao, Q., Sailor, D.J., Wentz, E.A., 2018. Impact of tree locations and arrangements on
845 outdoor microclimates and human thermal comfort in an urban residential
846 environment. *Urban For. Urban Green.* 32, 81–91.
847 <https://doi.org/10.1016/j.ufug.2018.03.022>

848 Zheng, S., Guldmann, J.M., Liu, Z., Zhao, L., 2018. Influence of trees on the outdoor
849 thermal environment in subtropical areas: An experimental study in Guangzhou,
850 China. *Sustain. Cities Soc.* 42, 482–497. <https://doi.org/10.1016/j.scs.2018.07.025>

851 Zhou, W., Wang, J., Cadenasso, M.L., 2017. Effects of the spatial configuration of trees
852 on urban heat mitigation: A comparative study. *Remote Sens. Environ.* 195, 1–12.
853 <https://doi.org/10.1016/j.rse.2017.03.043>